VI. Anatomy of the paranode-node-paranode region in the cat

by C.-H. Berthold and M. Rydmark

Section of Neuroanatomy, Department of Anatomy, University of Gothenburg, Box 33031, S-40033 Göteborg (Sweden), and Department of Anatomy, Karolinska Institutet, Box 60400, S-10401 Stockholm (Sweden)

Anatomically, nodes of Ranvier are those myelin-free, short, constricted and evenly distributed segments of a myelinated nerve fiber present at the meeting points of consecutive Schwann cells. The intervening myelinated and comparatively long fiber segments are referred to as internodes. Physiologically, nodes of Ranvier correspond to the only sites along a myelinated nerve fiber which support impulse conduction actively and are open to currents flowing between the axoplasm and the endoneurial space. Hence detailed knowledge of nodal anatomy is a necessary element for the full understanding of the phenomena on which the fast propagation of information in all higher vertebrates depend. Electron microscopy has revealed a far more complex structural organization at the mammalian node of Ranvier than is indicated by light microscopy. Ultrastructural observations thus suggest that not only the organization of the very nodal fiber segment is significant for nodal function but that also adjacent segments of the two meeting Schwann cells - the paranodes - might be involved in nodal activities (for references and reviews, see citations 1-5, 15, 18-20, 26, 27, 33).

The present communication deals exclusively with the ultrastructural anatomy of the paranode-node-paranode-(PNP)-region in feline spinal root fibers, and then mostly with large fibers (diameter (D) > 10 µm). It is our intention to give a rather strict anatomic presentation leaving out functional speculations. Morphometric data obtained from serially sectioned (n > 500) and reconstructed (n > 150) nodes will be emphasized[5,27]. It should be noted that the data given below represent what we refer to as 'tentative fresh-state' values as calculated from electron microscopic measurements using compensatory algorithms that account for various preparatory changes[7,8]. A brief summary of methods used is given before the legend to figure 1.

General description of the paranode-node-paranode-(PNP)-Region

A PNP-region consists of a central node of Ranvier and of the paranodes of the bordering internodes. The internodal fiber segments between consecutive PNP-regions are referred to as stereotype internodal (STIN) segments (fig. 1). For morphometric data of a large myelinated nerve fiber, see table.

The paranode

Paranodes are characterized by longitudinal myelin sheath furrows that, with increasing depth, extend to the node of Ranvier. Each furrow holds a column of Schwann cell cytoplasm that is rich in mitochondria, glycogen granules and lipid droplets. These mitochondrion-rich cords of the outer cytoplasmic Schwann cell compartment will in the following be referred to as 'mitochondrion bags' (fig. 1). It can be calculated that there are in an PNP-region of a large cat fiber roughly 20000 Schwann cell mitochondria ~ 0.5 µm long and ~ 0.15 µm in diameter[6]. This value should be compared to the 1100-1600 mitochondria of a liver cell[22]. Often the nodal extremities of the mitochondrion bags contain large amounts of round or oblong moderately electron dense single membrane bounded bodies 50-200 nm × 30-500 nm in size. These bodies are referred to as Schwann cell juxta-nodal bodies. Their functional significance is obscure.

Paranodal length increases with fiber diameter from 5-10 µm to 50-80 µm. The paranode lacks Schmidt-Lantermans insicures and can be subdivided in a) a main segment and b) an end segment. It should be noted that the term paranode in a number of recent publications[21,34,36] dealing with freeze-etched nerve fibers has been used in a restricted sense only denoting the paranodal end segment.

a) Paranodal main segment

This part of a paranode is, due to the crenation of the myelin sheath, characterized by a fluted axon. The fluting becomes increasingly deeper in the nodal direction and ceases abruptly close to the paranodal end segment. As a consequence, all fiber compartments, except the axonal one, increase gradually in cross section area till the end segment is nearly reached. The axonal reduction takes place in 2 steps: a first gradual decrease to 75-50% of the STIN-value and a second abrupt decrease to an area that is 10-20% of the original one[1,26]. This reduction of the cross-section of the axoplasmic core conductor means that the current density during impulse conduction increases 5-10 times close to a node of Ranvier. A comparison in these respects between dorsal and ventral root PNP-regions shows that the higher value should be valid for afferent fibers and the lower value for efferent ones[26].

The ultrastructure of the periaxonal space and of the axolemma in the paranodal main segment is similar to that noted elsewhere in the STIN-segment[3,4]. Thus the axolemma and the adjacent Schwann cell plasma membrane either form 5-layered membrane complexes similar to tight-junctions or 7-layered membrane complexes, the central layer, i.e. the periaxonal

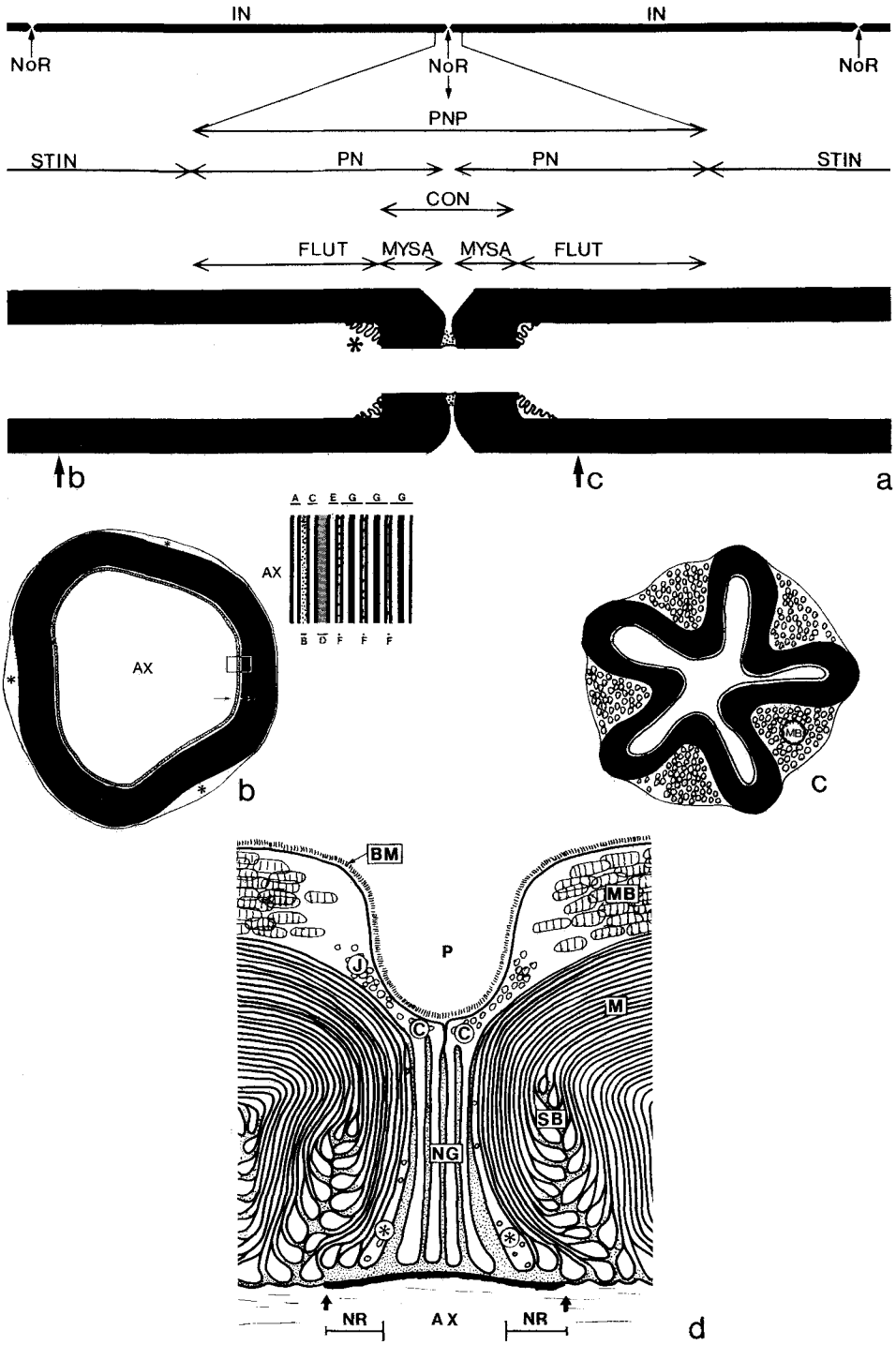

Figure 1. Schematic drawing introducing the terminology used in the running text. *a* CON = constricted axon segment. Asterisk indicates axon-Schwann cell network. FLUT, paranodal main segment characterized by a fluted axon (see fig. 1,c); IN, internode; MYSA, paranodal end segment characterized by the myelin sheath attachment to the axolemma; NoR, node of Ranvier; PNP, paranode-node-paranode region; STIN, stereotype internodal region. *b* Cross sectioned STIN region. Asterisks indicate the outer cytoplasmic Schwann cell compartment. The periaxonal space (arrows) is stippled and demarcated by the axon (Ax) and the inner cytoplasmic Schwann cell compartment (light layer in the figure). A magnified part of the boxed area is shown just to the upper right of fig. 1,b. The detail describes membrane arrangements that separate the axoplasm (Ax) from the compact myelin. A, axolemma (~ 9 nm); B, periaxonal space (0–5 nm), stippled; C, inner Schwann cell membrane (~ 8 nm); D, Schwann cell cytoplasmic layer (3–5 nm); E, outer Schwann cell membrane (~ 8 nm); C+D+E, inner cytoplasmic Schwann cell compartment; F, intramyelin fluid or extracellular space (~ 1 nm); G, myelin lamella (17–18 nm). *c* Cross sectioned main paranodal segment. MB, mitochondrion bag. *d* Median longitudinal section through node of Ranvier. Ax, axon; BM, Schwann cell basement membrane; C, nodal collar, the 2 meeting collars in the picture constitute the outer demarcation of the nodal Schwann cell compartment. J, juxta nodal Schwann cell bodies; M, myelin sheath; MB, mitochondrion bag; NG, nodal gap; NR, nodal gap recessus; P, perinodal space; SB, ear-of-barley like representation of a pile of crosscut turns of the terminal cytoplasmic cord (TCC), which forms the spinous bracelet (of Nageotte). Small arrows indicate the extent of the nodal axolemma. Stippling denotes the periaxonal space outside the MYSA and nodal axon segments (the extracellular space of the nodal gap is considered to be a part of the periaxonal space). Asterisks mark out the nodal gap walls.

space being 2–4-nm-thick. A periaxonal space of 10–20 nm, the width commonly reported in araldite or epon embedded specimens[17,19,28] has not been observed in large cat fibers after embedding in Vestopal-W or in glycol methacrylate, the latter medium being water soluble[1–5,7]. In large mammalian fibers tracer molecules that enter the nodal gap and/or the outer mesaxon from the endoneurial space do not seem to reach the periaxonal space of the STIN- and paranodal main segments[16,17].

The inner cytoplasmic Schwann cell compartment terminates at the nodal end of the paranodal main segment. In many paranodes the more nodal parts of some axonal crests disintegrate and form winding tubular processes that are embedded in expansions of the inner cytoplasmic Schwann cell compartment. This is the axon-Schwann cell network, a component of the normal paranode that becomes more prevalent with increasing age[1,31].

b) Paranodal end segment

The length of this segment does not depend on fiber size and measures 3–4 μm in all fibers[2]. The segment is characterized by the termination of the myelin sheath and by the attachment of the myelin to the narrow cylindric axon of the paranodal end segment, the diameter of which is ½–⅓ of that noted in the STIN-region[26]. This part of the axon will be referred to as the MYSA (myelin sheath attachment) axon segment. The two MYSA axon segments of meeting internodes and the intervening nodal axon segment make up the constricted (CON) axon segment of a PNP-region. The CON-segments show several unique features that may be significant when trying to integrate structural organization and function of the node of Ranvier.

In a median longitudinal section (fig. 5) the end of each terminating myelin lamella appears split into 2 leaflets which enclose a drop-shaped amount of Schwann cell cytoplasm forming a so-called terminal cytoplasmic pocket. The whole set of pockets seen in an end segment represents the cross-sectioned appearance of one single continuous and narrow cord of Schwann cell cytoplasm that encircles the axon in a complex helical manner. Each turn of this terminal cytoplasmic cord (TCC) corresponds to the termination of 1 myelin lamella. A TCC of a large fiber is about 2000–3000 μm in length, ~0.1 (0.07–0.15) μm in diameter, 20–25 μm^3 in volume and has a mantle area of 700–1000 μm^2. The TCC interconnects the inner and outer cytoplasmic Schwann cell compartments via the nodal gap walls, the nodal collars and the mitochondrion bags. Thus the TCC is structurally an equivalent to the cytoplasmic spiral of an incisure of Schmidt-Lanterman. It should, however, be noted that the cytoplasmic cord of the incisure is more than twice as long as the TCC (6600 μm vs 2530 μm) in our large standard fiber (table). So, there is a much shorter distance between the outer and inner cytoplasmic Schwann cell compartments at the node than elsewhere internodally. This is the consequence of the smaller diameter of the MYSA-axon.

That turn of the TCC which belongs to the innermost myelin lamella attaches to the axolemma of the MYSA axon furthest from the node. Subsequent lamellae then terminate in consecutive order up to the node. However, only 10–20% of these lamellae attach directly to the axolemma via turns of the TCC. Those turns of the TCC which belong to the remaining 80–90% of the myelin lamellae coil up on top of one another in sets of 10–25 turns. In a longitudinal section this gives the picture of 'ear-of-barley' like aggregations of terminal cytoplasmic pockets (fig. 6) that reach 0.5–1.5 μm into the surrounding compact myelin. The turns of the TCC which belong to the 3–10 outer- and inner-most myelin lamellae contain a diffuse material of low contrast. Intervening turns, i.e. 80–90% of the TCC contains a more electron-dense material rich in high density granules 2–4 nm in size. The presence of the TCC and its arrangement outside the MYSA axon explains the so-called spinous bracelet or cuff of Nageotte: those coils of the TCC which attach to the axolemma constitute the very cuff and those grouped together in what can be referred to as supracoils constitute the spines. The turns of the TCC which reach to the axolemma are attached to it by gap junction-like membrane complexes. The intervening periaxonal space is 3–5 nm thick and at least in its more nodal parts, open to the nodal gap[28]. The turns of the TCC are joined together by a system of more or less continuous tight junctions[28]. One set of these tight junctions may seal off the periaxonal space and its helical continuations into the spinous cuff from the intramyelin fluid space. Unless there is such a seal the 17300 μm^3 of the intramyelin fluid space communicates with the periaxonal space via a total crossection area that is about 6 μm^2 in the paranodal end segment and about 7.5 μm^2 in the STIN segments.

The volume of the periaxonal space of the paranodal end segment is not known and difficult to calculate. Assuming that the TCC is surrounded by a layer of the periaxonal space that is 2–3 nm thick, an approximation that is realistic in view of the electron microscopic picture (fig. 6), it can be calculated that the end segment holds a total periaxonal space of ~20 μm^3. Since the mantle area of the MYSA axon is ~60 μm^2 it should face ~10 times as much periaxonal space per unit membrane area than the rest of the internodal axolemma. A comparison between the Schwann cell membrane area facing the periaxonal space of the end segment and the membrane area of the MYSA axon shows a Schwann cell/axon ratio of ~13 (800/60). Elsewhere internodally, this ratio is 1. The turns of the TCC of the outermost 2–4 myelin

lamellae do not attach to the axolemma but are separated from it by an interspace about 20–50 nm in width thus forming the ceiling of the nodal gap recessus (fig. 1). The most nodal turn of the TCC is particularly large and 'high'. It constitutes one of the two nodal gap walls. It often contains large numbers of juxtanodal Schwann cell bodies.

The paranodal end segment offers a rather spectacular ultrastructural organization. First, there is a system of narrow spiralling extra and intracellular spaces, the former, i.e. the periaxonal space, is connected to the nodal gap and the latter, i.e. the TCC is connected to the mitochondrion bags and via the nodal brushborder to the extracellular space of the nodal gap and to the immediate surroundings of the nodal axolemma. Second, the axolemma of the MYSA segment and the Schwann cell plasma membrane of the TCC exhibit intriguing arrays of intramembranous particles (see article by Rosenbluth).

The node of Ranvier

This part of the PNP-region is surrounded by the perinodal space, i.e. by that part of the endoneurial space that reaches in between the ends of the meeting internodes (figs 2 and 5). The space is conspicuous in large fibers. The Schwann cell layer that borders the perinodal space is rich in juxta nodal bodies and shows a plasma membrane equipped with coated cup-like impressions, inside arrays of electron-dense granules and sometimes with small tufts of microvilli[1]. According to classical physiological concepts the perinodal space should be the immediate source for and the recipient of ions moving into and out from the node of Ranvier.

The node of Ranvier can be described as consisting of 2 concentrically arranged compartments: A) an outer Schwann cell compartment and B) an inner axon compartment.

A) The Schwann cell compartment

This compartment can be separated in 3 regions: 1. the outer demarcation region, 2. the nodal gap and 3. the nodal gap walls (see figs 1 and 5).

1. The outer demarcation of the node of Ranvier is given by more or less overlapping extensions of the outer cytoplasmic Schwamm cell compartments of the two meeting internodes (figs 7 and 8). These extensions are called the nodal collars. The nodal collars send a brushborder of radially arranged microvilli into the subjacent nodal gap. The brushborder is as a rule well developed at those sectors of a nodal collar which are direct continuations of a paranodal mitochondrion bag. Here a collar emits tufts of long microvilli. Intervening sectors emit fewer and shorter microvilli. A tuft-like distribution of the nodal Schwann cell brushborder is particularly striking in very large fibers (fig. 2). The presence of coated invaginations in the plasma membrane of the nodal collars between the emerging microvilli indicates active transport between the Schwann cell and the extracellular space of the nodal gap.

In some sectors of an outer demarcation region the nodal collars of the 2 meeting Schwann cells overlap and are joined by 5-layered membrane complexes similar to tight junctions. To this are added in many nodes clumps of apparently extracellular lamellar material (figs 7 and 8). In other sectors of the same node the collars are small and separated by an opening 0.1–0.2 μm in width. At such sites the content of the nodal gap is separated from the perinodal space only by the Schwann cell basement membrane. As a whole the demarcation region consists of alternating openings and closures. The total area of the openings in an outer nodal demarcation region can, when accounting for preparatory changes, be approximated to 0.2–0.5 μm^2.

2. The nodal gap appears, when viewed in a median longitudinal section like a narrow isosceles trapezoid of which longer and shorter bases face the nodal axolemma and the nodal collars, respectively, and which slanting sides are formed by the nodal gap walls (fig. 5). The gap contains the nodal microvilli of the Schwann cell suspended in the nodal gap matrix substance (figs 3 and 4). The latter occupies the extracellular space of the nodal gap and consists of a mucopolysaccaride with the properties of a cation exchanger[20]. The blunt ends of the microvilli end less than 5 nm from the nodal axolemma. From the ultrastructural point of view (7–8 microfilaments per microvillus and no terminal web) the nodal gap brushborder appears to be more related to the brushborder of the proximal tubules in the kidney than to that of the intestinal epithelium. A nodal gap of a large fiber contains 800–1000 microvilli 70–80 nm in diameter and ~ 1 μm of mean length which gives a total microvillus membrane area of about 200 μm^2.

The nodal gap forms low recesses that extend proximally and distally along the axon under the myelin for a distance of 0.1–0.4 μm. The nodal gap recesses, which contain only nodal gap substance and no microvilli, are 20–50 nm high and overhung by the most nodal turns of the TCC of the paranodal end segment. The Schwann cell membrane area facing a nodal recesses is about 10 μm^2.

As discussed elsewhere[7] it seems likely that dehydration submits the nodal region to forces of shrinkage that tear apart the internodes thus opening up the nodal gaps. This would mean that estimations of nodal gap volumes as based on direct measurements in electron micrographs would give too large values. If it is assumed that the nodal microvilli in the fresh state are arranged in a radial hexagonal array of maximal close packing (see figs 3 and 4) the microvilli volume would make up 90% of the total gap volume;

the remaining 10% would be accounted for by the extracellular space of the nodal gap. From this assumption it can be calculated that the extracellular space in the nodal gap of a large fiber is a total of 0.5–0.6 μm^3 of which ~ 50% occupies the nodal recesses. In this way the nodal gap extracellular space makes up but 10% of the total extracellular space that relates directly to the axolemma of the whole constricted axon segment. The progression of the nodal gap extracellular volume with fiber size is shown in figure 12.

3. The nodal gap walls, called the proximal and the distal wall with reference to the neuronal soma, are each formed by the most nodal turn of the TCC. Some walls contain large numbers of juxta nodal Schwann cell bodies. The membrane area of a nodal gap wall facing the nodal gap extracellular space is 25–50 μm^2.

Thus the 2 Schwann cells that consitute the outer compartment of the node of Ranvier face the nodal gap extracellular space with a total membrane area of about 250 μm^2 (fig. 11). Approximately 75%, 20% and 5% of this area are provided by the brushborder, the nodal gap walls and the 'ceiling' of the nodal recesses, respectively. This means that the nodal Schwann cell membrane per area unit is related to a layer of the nodal gap extracellular space that is on the average 2–3 nm thick, i.e. about the same value as noted for the average thickness of the periaxonal space in relation to both the inner cytoplasmic Schwann cell compartment and to the TCC.

B. The axonal compartment

This part of the node of Ranvier consists of the nodal axon segment (fig. 2). The segment is more or less barrel shaped. Its midpoint diameter is a few percent larger than the diameter of the bordering MYSA segments. It is demarcated from the nodal gap by the nodal axolemma. The nodal axolemma is that ~ 1-μm-wide strip of axon plasma membrane which, carrying a layer of electron-dense material on its axoplasmic side, extends between the 'last' closely attached turn of the TCC of a proximal internode and the 'first' closely attached one of the consecutive distal internode (fig. 5). Electron microscopically the nodal axolemma shows minor pointed irregularities, < 30 nm in height and separated by 50–100 nm (fig. 9). These irregularities increase the length of the axolemma contour with ~ 7% (SD = 3%) and ~ 16% (SD = 5%) in cross sections and in median longitudinal sections, respectively, thus increasing the membrane area of the nodal axolemma with ~ 24%[5].

There is a complete layer of electron-dense material, about 30 nm thick, inside the nodal axolemma in all fibers except the smallest ones (< 3–4 μm in diameter). In such fibers the few microvilli present seem to be in contact only with those parts of the axolemma that carry the inside electron-dense material. At high magnification in very thin sections of vestopal-embedded fibers the electron-dense material resolves into a meshwork of round electron lucent spaces 10–20 nm in size and an intervening electron opaque substance. In GMA-embedded specimens the inside axolemmal coating is 80–100 nm thick (fig. 5). Evidently, aceton dehydration and vestopal-embedding removes a substantial part of the material present originally.

The axolemma of several nodes shows spine- and crest-like outgrowths. The nodal crests, run across the longitudinal axis of the axon, and measure 0.1–0.6 μm in height, 0.05–0.4 μm in width and 1–4 μm in length. The nodal spines show a centrifugal tapering and in cross section are more or less circular (fig. 9). They measure 50–100 nm in diameter and 50–500 nm in height.

The area of the nodal axolemma develops with fiber size from ~ 4 μm^2 in small to about 30 μm^2 in large fibers. The progression seems to be exponential or to follow 2 connected linear distributions of different slopes: the lesser slope noted in fibers less than ~ 10 μm in diameter (fig. 10). When present, nodal outgrowths, like crests and spines, seldomly form more than 10% of the total area.

The nodal axolemma can be separated into 2 main territories. One faces the microvilli containing part of the nodal gap. The other faces the empty-looking nodal recesses. The relative size of the latter increases with increasing fiber size from ~ 25% in small fibers to ~ 50% in large ones. In a large fiber, this means that ~ 50% of the total nodal axolemma are related to the nodal recesses, that ~ 45% are covered by the tips of the Schwann cell microvilli and that ~ 5% are covered by the intervening nodal gap matrix substance.

Large ventral root fibers have a nodal membrane area that is relatively larger than that of large dorsal root fibers. Our data (fig. 10) indicate that the nodal axon membrane area of a ventral root fiber is about 25% larger than that of a dorsal root fiber of the same thickness. This difference between the nodal regions of efferent and afferent fibers of equal calibre might be of significance for the functional differences as noted between motor and sensory fibers – for instant differences in the rate of accomodation, in the K^+-conducting system, in the Na^+-inactivation curve and in the kinds of K^+-channels[14,24,30,33,35].

Figure 13 shows a plotting of the ratio between the membrane area of the Schwann cell facing the nodal gap and that of the nodal axon. Both in ventral and dorsal roots the ratio increases rapidly from 2–3 in the smallest fibers and reaches a maximum of 15 in fibers about 10 μm in diameter. Further increase in fiber size means a decrease in the ratio down to 6–7 in the largest fibers. If it is assumed that the Schwann cell

All electron micrographs show nerve fibers from glutaraldehyde (5%) perfusion fixed adult cats. The lumbosacral spinal roots were osmicated, Vestopal-W embedded or glycol-methacrylate (GMA) embedded, and serially sectioned. The sections were double stained with lead citrate and uranyl citrate and examined in a Philips EM 301 electron microscope. (For a detailed description of the preparative procedures, see references 1, 5, 7, 8, 27).

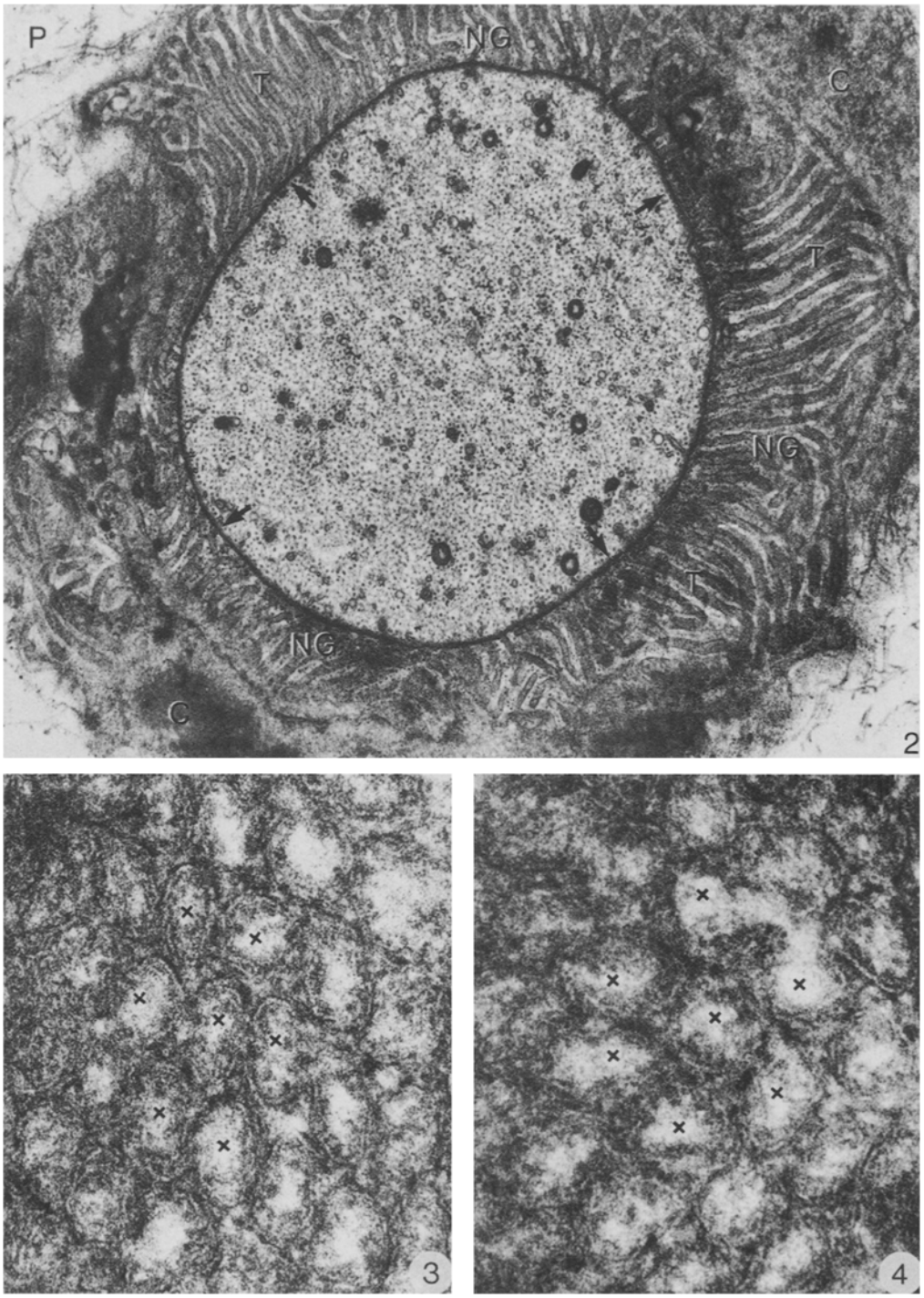

Figure 2. Electron micrograph showing a cross section of a node of Ranvier of a large ventral root nerve fiber. The nodal axolemma carries a continuous electron dense undercoating (small arrows). The Schwann cell microvilli of the nodal gap (NG) are arranged in three major tufts (T). The nodal gap is demarcated from the perinodal space (P) by the Schwann cell collars (C) of the nodal gap. Vestopal embedding. × 18080. (From Berthold and Rydmark[5]).

Figures 3 and 4. Electron micrographs showing cross sectioned Schwann cell microvilli of the nodal gap of a longitudinally sectioned node of Ranvier of a large nerve fiber. The nodal axon is outside the sectioning plane. Fig. 3 shows a section from the mid-level of the nodal gap, while Fig. 4 shows a section close to the nodal axon. Note the hexagonal close-packing of microvilli (x). GMA embedding. × 140000. (From Berthold and Rydmark[5]).

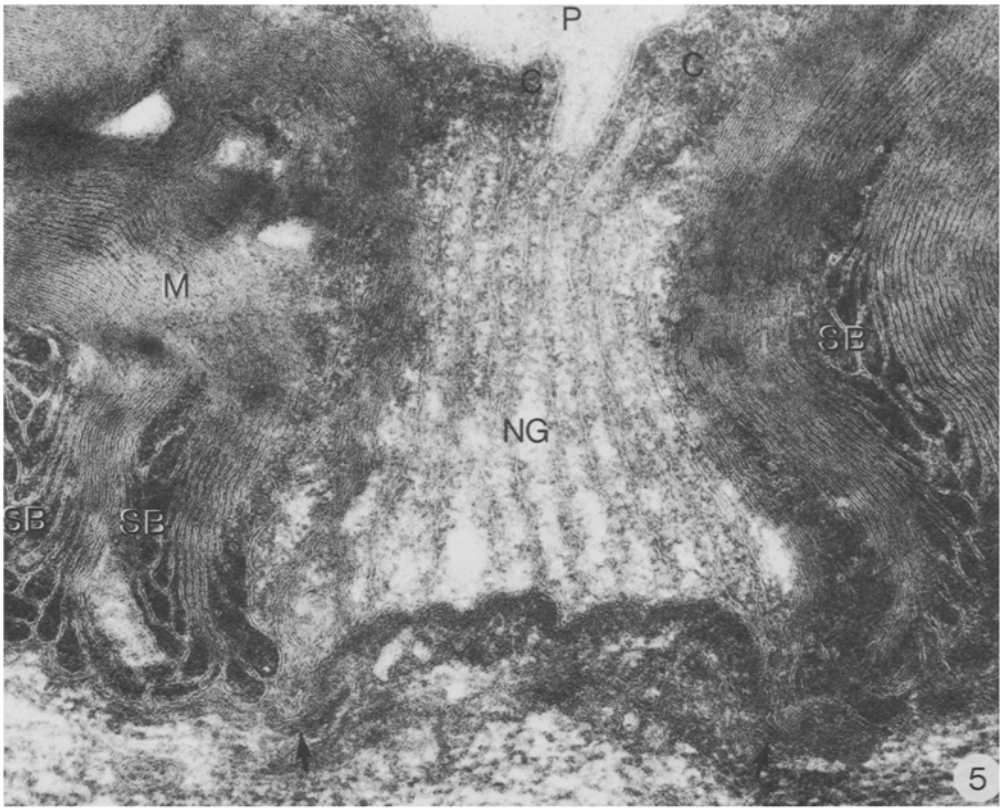

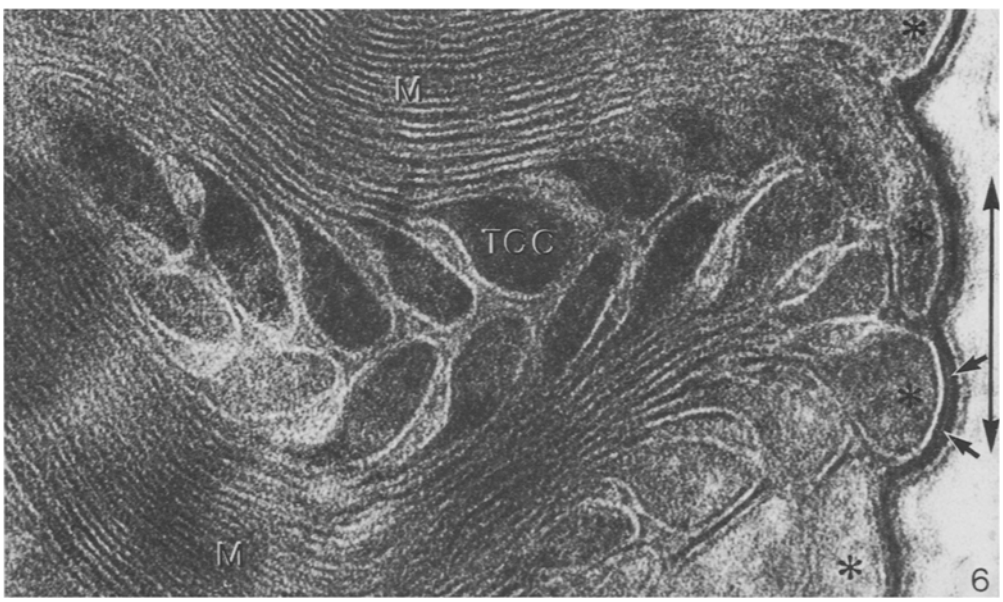

Figure 5. Electron micrograph showing a longitudinal section through the nodal gap of a large ventral root nerve fiber. The nodal axolemma extends between the 2 arrows. Note the comparatively thick undercoating of the nodal axolemma. The nodal gap (NG) is filled with densely packed Schwann cell microvilli. M, myelin sheath; P, perinodal space; C, nodal Schwann cell collars; SB, part of spinous bracelet. GMA embedding. × 56000. (From Berthold and Rydmark[5]).

Figure 6. Electron micrograph showing a part of a spinous bracelet of a longitudinally sectioned paranodal endsegment (see fig. 5). Large 2-headed arrow indicates the length axis of the axon. Coils of terminal cytoplasmic cord (TCC) give an ear-of-barley like configuration. A few of the TCC coils attach to the axon (asterisks). Note the thin light rim (small arrows) representing the periaxonal space. Vestopal embedding. × 168000.

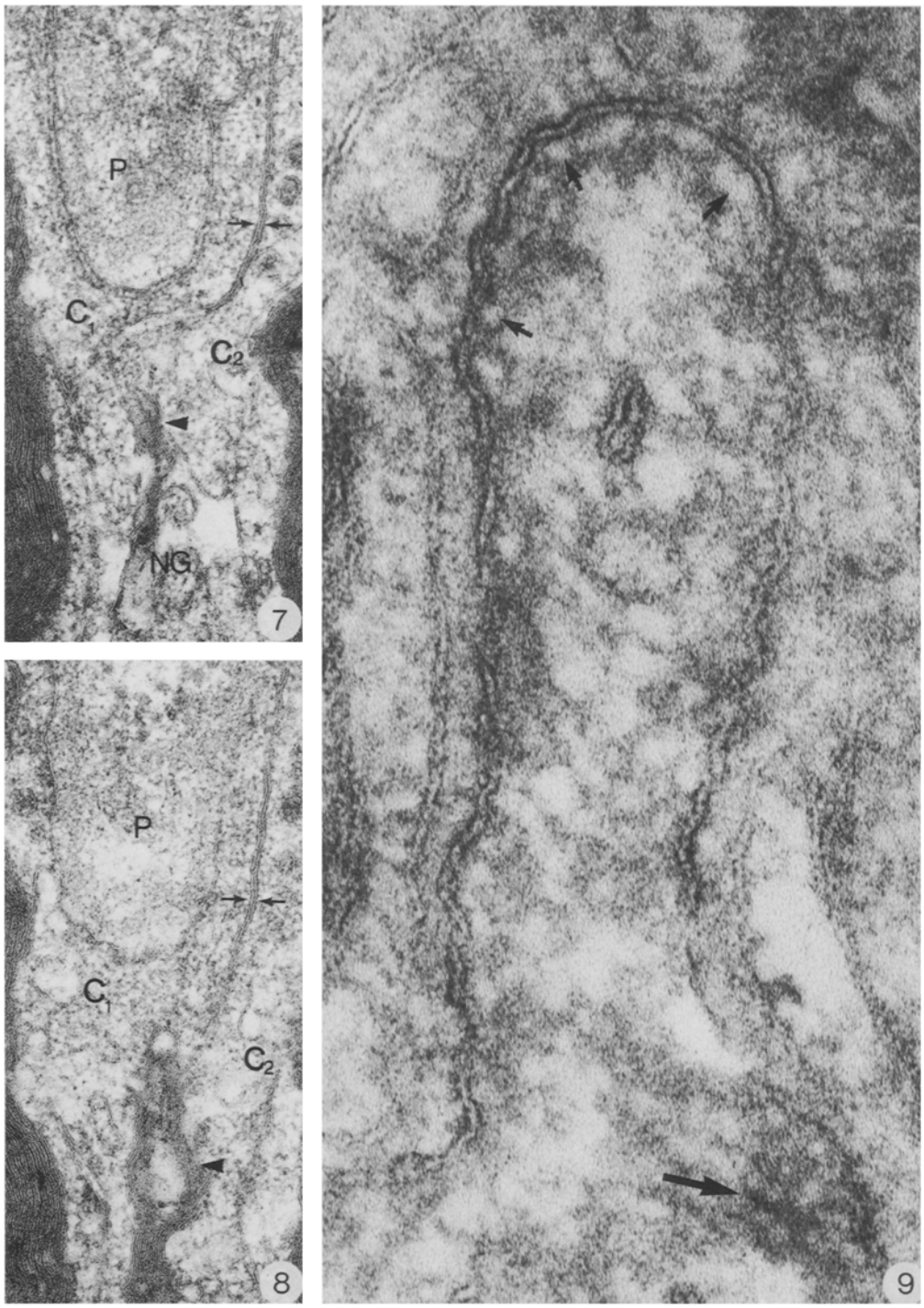

Figures 7 and 8. Electron micrographs showing longitudinal serial sections (3 sections apart) of the outer aspect and demarcation of the same nodal gap of a large ventral root nerve fiber. One nodal collar (C_1) covers the nodal gap and the collar (C_2) of its neighbor Schwann cell with a delicate cytoplasmic tonge that continues its extent up the perinodal wall of its neighbor Schwann cell. The meeting Schwann cell membranes form 5-layered complexes (arrows) suggesting a tight-junction contact. Between the overlapping C's and the nodal gap proper there is a dark lamellar body (large arrow heads). Vestopal embedding. $\times 60000$. (From Berthold and Rydmark[5]).

Figure 9. Electron micrograph showing a nodal spine, i.e. a spinous outgrowth of the nodal axon, in a longitudinal section of a large dorsal root nerve fiber. Immediately inside the axolemma there are at severeal sites (small arrows) round lucent spaces 10–20 nm in diameter and demarcated by a diffuse electron dense material. This arrangement is also illustrated in the tangentially cut part of the axolemma as marked out by the large arrow. Vestopal embedding. $\times 24000$. (From Berthold and Rydmark[5]).

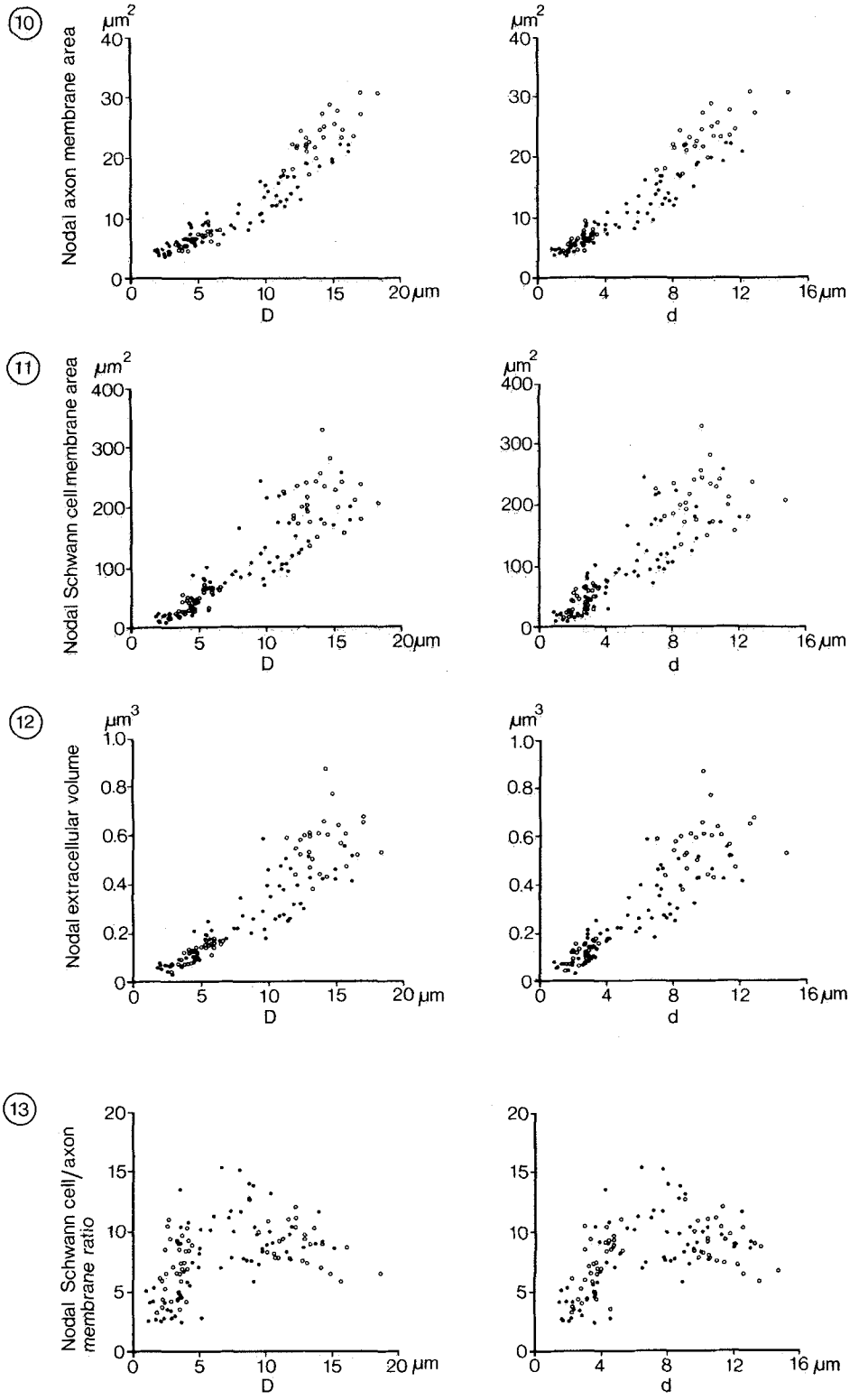

In figures 10–13 tentative fresh-state values of some nodal variables, as estimated from serial section reconstructions, have been plotted against nerve fiber diameter (D) and internodal axon diameter (d). ○, Ventral roots; ●, dorsal root. (From Rydmark and Berthold[27]).

Fig. 10. The membrane area of the nodal axolemma plotted against D and d. Fig. 11. The Schwann cell membrane area in the nodal gap plotted against D and d. Fig. 12. The extracellular volume of the nodal gap plotted against D and d. Fig. 13. The ratio, between the Schwann cell membrane area in the nodal gap (see fig. 11) and the membrane area of the nodal axolemma (cf. fig. 10), plotted against D and d.

via its plasma membrane in the nodal gap controls the composition of the extracellular fluid of the nodal gap, a composition that presumably depends on constituents that are delivered into the nodal gap or removed from it, it is reasonable that the higher the Schwann cell/neuron-membrane area ratio, the more effectively will the milieu directly outside the nodal axolemma be controlled. With this background it is noteworthy that nerve fibers of α-motor neurons characterized by tonical activity with a high probability are to be found in the fiber calibre spectrum interval of 10–15 µm, whereas motor neurons characterized by phasical activity should be represented by the thickest fibers in the ventral root, as can be calculated from the conduction velocities[10–12].

The size of the periaxonal space outside the nodal axolemma calculated as an evenly thick layer of the nodal gap extracellular space is ~30 nm, i.e. roughly the same as estimated for the periaxonal space outside the MYSA-axon segments. Thus, in a large myelinated nerve fiber the periaxonal space forms a ~3-nm-thick layer outside the STIN- and the paranodal main-axon segments. Outside the MYSA- and the nodal axon-segments the periaxonal space increases by about one order of magnitude as does the Schwann cell membrane area facing the same periaxonal space. These relations together with the multitude of intramembraneous particles in the axolemma of the constricted axon segment suggest that not only the nodal axon segment but the whole constricted axon segment together with its Schwann cell surroundings should be taken into consideration when discussing the correlation between neurophysiological properties and structural organization of the node of Ranvier.

No full description of the nodal axoplasm and its contents will be given in the present communication. In short, the nodal axoplasm contains the same formed elements as elsewhere internodally but at a higher concentration. There is no particular aggregation of axonal mitochondria in relation to the nodal axolemma[4].

Hypothetical intra-, extra- and trans-cellular communication pathways at the node of Ranvier

The presented ultrastructural organization at the node of Ranvier offers several hypothetical routes for ionic flow between the axon and the 'external solution', i.e. the perinodal and/or endoneurial spaces. All these routes are considered to be bidirectional.

A) The classic or direct, nodal, route

This is the route of conventional saltatory conduction theory. Here the nodal axolemma is the only structural entity recognized to be of functional interest: ionic currents pass the nodal axolemma bidirectionally between the axoplasm and the outer solution, i.e. the endoneurial, space via a 'wide open' nodal gap. In terms of a 'fresh state' large cat node, this would mean a pathway through the very much restricted nodal gap extracellular space inbetween the microvilli, further on through the minute openings in the outer nodal demarcation between the nodal collars (~0.2 µm^2, cf. table) and finally through the Schwann cell basement membrane. According to our 'fresh state' model the current density at the outer nodal gap demarcation should be 30–100 times that close to the nodal axolemma.

In spite of the narrow area open to diffusion through the nodal gap it can be calculated, assuming that the nodal gap matrix substance has the diffusion properties of a weak K^+-solution, that for instance K^+-ions diffuse out from the node freely enough not to interfere with the restitution of the membrane potential[27]. In this context it is interesting to note that the resistance offered by the nodal gap extracellular space of our 'fresh state' modell is 0.5–2 MΩ as calculated from a resistivity of ~100 Ω cm^{-1}, i.e. from the resistivity of the external solution as given by neurophysiology[32]. A resistance of 0.5–1.0 MΩ corresponds to the serial resistance noted in clamp-experiments on rabbit and rat nodes[9,23].

B) The node-paranodal route

This route is suggested by the ultrastructural organization of the nodal Schwann cell compartment and its connection to the paranodal mitochondrion bags. It has thus been suggested, in analogy with the function of other epithelial cells equipped with a brushborder and rich in mitochondria (such as the cells of the avian salt gland, and the cells of the proximal tubules of the kidney) that the Schwann cell may control the ionic milieu of the nodal gap extracellular space. An active control of both Na^+ and K^+ fluxes[5,18,27,29] has been suggested.

The node-paranodal route passes over the nodal axolemma to the nodal gap extracellular space, through the Schwann cell plasma membrane of the nodal gap (~250 µm^2, see table; the major part of this area being offered by the microvilli) into the mitochondrion-rich paranodal Schwann cell cytoplasm and reaches finally the endoneurial space via passage through the Schwann cell plasma and basement membranes. It is noteworthy that this route uses an area of communication between a nonaxonal compartment and the nodal gap extracellular space that is ~3 orders of magnitude as large as that of the direct nodal route.

C) Additional routes

As hinted above, morphometry and freeze etching studies of the paranodal end segments indicate that not only the nodal axon segment but also the MYSA segments might be involved in the ionic shifts behind

Morphometric data of a PNP-region of a large myelinated nerve fiber

General fiber characteristics: Fiber diameter (D) = 17.5 µm
Internodal axon diameter (d) = 12.5 µm
Number of myelin lamellae (nl) = 140
Myelin sheath thickness (M) = 2.5 µm
g-(d/D)-value = 0.7
Internodal length = 1800 µm
The data of this table are taken from, or derived from literature references 1–8, 26, 27

Paranode (values are given for 1 of the 2 paranodes of a PNP-region)		*
Paranodal main segment		
Segment length	75 µm	(4%)
Axon, minimum cross section area	70 µm²	(57%)
Axon, mean cross section area	102 µm²	(83%)
Axon, maximum circumference	63 µm	(160%)
Axon, mean circumference	49 µm	(125%)
Axon, membrane area	3680 µm²	(5%)
Axon, volume	7650 µm³	(3.5%)
Periaxonal space, cross section area	0.2 µm²	(125%)
Periaxonal space, volume	15 µm³	(5%)
Fiber, maximum cross section area	289 µm²	(120%)
Fiber, maximum circumference	63 µm	(115%)
Myelin sheath, maximum cross section area	188 µm²	(160%)
Myelin sheath, maximum circumference	88 µm	(160%)
Schwann cell inner cytoplasmic compartment, maximum cross section area	0.25 µm²	(160%)
Schwann cell outer cytoplasmic compartment maximum cross section area	28 µm²	(230%)
Intramyelin fluid space, maximum cross section area	12 µm²	(160%)
Schwann cell membrane area facing the axon	3680 µm²	(5%)
Schwann cell membrane area facing the endoneurial space	4330 µm²	(5%)
Myelin membrane area	578000 µm²	(5%)
Schwann cell inner cytoplasmic compartment volume	15 µm³	(5%)
Schwann cell outer cytoplasmic compartment volume	1214 µm³	(6%)
Myelin sheath volume	10400 µm³	(5%)
Intramyelin fluid space, volume	867 µm³	(5%)
Schwann cell mitochondria, maximum number per cross section	400	
Schwann cell mitochondria, total number	~ 10000	
Paranodal end segment		
Segment length	4 µm	(0.2%)
Axon diameter	4.75 µm	(38%)
Axon cross section area	17.7 µm²	(14%)
Axon circumference	14.9 µm	(38%)
Axon membrane area	60 µm²	(0.08%)
Axon volume	71 µm³	(0.03%)
Periaxonal space cross section area	0.6 µm²	(38%)
Periaxonal space volume	2.4 µm³	(0.08%)
Terminal cytoplasmic cord, number of turns	140	
Terminal cytoplasmic cord, number of turns attached to axon	26	
Terminal cytoplasmic cord, length	2530 µm	
Terminal cytoplasmic cord, diameter	0.1 µm	
Terminal cytoplasmic cord, cross section area	0.008 µm²	
Terminal cytoplasmic cord, membrane area	795 µm²	
Terminal cytoplasmic cord, volume	20 µm³	
Terminal cytoplasmic cord, attachment area to axon	55 µm²	
Terminal cytoplasmic cord, mean diameter of turns	5.75 µm	
Terminal cytoplasmic cord, volume inbetween turns not attached to axon	18 µm³	
Myelin sheath membrane area	14200 µm²	(0.1%)
Myelin sheath volume	260 µm³	(0.1%)
Intramyelin fluid space, cross section area	6 µm²	(80%)
Intramyelin fluid space, volume	22 µm³	(0.1%)
Schwann cell outer cytoplasmic compartment, cross section area	8 µm²	(65%)
Schwann cell outer cytoplasmic compartment, volume	32 µm³	(0.2%)
Schwann cell membrane area facing the endoneurial space (incl. the perinodal space)	200 µm²	(0.3%)
Node		
Schwann cell compartment (values represent contribution of 2 Schwann cells)		
Outer demarcation region		
Extracellular interconnecting area between the nodal gap and the perinodal space	0.2 µm²	
Hight, i.e. thickness of the Schwann cell collars	0.1 µm	
Nodal gap		
Width at the outer level	0.23 µm	
Width at the intermediate level	0.27 µm	
Width at the inner level	0.32 µm	
Hight (radial)	1 µm	
Extracellular mantle area at the outer part	0.5 µm²	
Volume	5.1 µm³	
Extracellular volume	0.7 µm³	
Extracellular volume in nodal gap racesses	0.3 µm³	
Extracellular volume in between microvilli	0.4 µm³	
Extracellular communication area between a nodal gap recessus and main nodal gap	0.5 µm²	
Schwann cell microvilli, number	800	
Schwann cell microvilli, mean length	1 µm	
Schwann cell microvilli, mean diameter	84 nm	
Schwann cell microvilli, total cross section area	4.4 µm²	
Schwann cell microvilli, total membrane area	210 µm²	
Schwann cell microvilli, total volume	4.4 µm³	
Nodal gap walls		
Schwann cell membrane area, walls	43 µm²	
Schwann cell membrane area, ceilings of nodal gap recesses	11 µm²	
Schwann cell cytoplasmic volume	4.3 µm³	
Cytoplasmic communication area (radial) in the walls	3–4 µm²	
Axonal compartment		
Axon length	1 µm	(0.006%)
Axon diameter	5.0 µm	(40%)
Axon cross section area	20 µm²	(16%)
Axon circumference	16 µm	(40%)
Axon membrane area	24 µm²	(0.03%)
Axon volume	19 µm³	(0.009%)

* Values in brackets represent the percentage of the total internodal value.

impulse propagation. There are several hypothetical routes of communication between the MYSA-axon segment and its periaxonal space on the one hand and other compartments in the surroundings on the other.

1. Communication in the nodal direction with the nodal gap extracellular space via the periaxonal space outside the MYSA axon segment (communication cross section area = $\sim 0.6\ \mu m^2$).

2. Communication in the internodal direction with the periaxonal space outside the rest of the internodal axon segment. This route is probably closed by tight junctions[25,28].

3.Communication with the intramyelin extracellular space. The route is probably closed by tight junctions[25,28].

4. Communication with the nodal and with the outer paranodal Schwann cell compartments via the TCC. This route implies passage through the Schwann cell plasma membrane of the TCC. The route has been suggested as a possible pathway for Na^+-ions that have been pumped out from the nodal axon through the nodal axolemma, reabsorbed into the Schwann cell by its nodal brushborder and returned to the immediate vicinity of the axolemma of the MYSA axon segment by transportation in the TCC[13,37]. Among the points of this hypothesis which are difficult to imagine is a current passing in the TCC wherein electrical resistance can be calculated to $\sim 300\ G\Omega$.

Acknowledgment. This work was supported by the Swedish Medical Research Council; Project No. 03157.

1 Berthold, C.-H., Ultrastructure of the node-paranode region of mature feline ventral lumbar spinal root fibers. Acta Soc. Med. upsal. *73* (1968) suppl. 9, 37–70.

2 Berthold, C.-H., Ultrastructure of postnatally developing peripheral nodes of Ranvier. Acta Soc. Med. upsal. *73* (1968) 145–168.

3 Berthold, C.-H., Morphology of normal peripheral axons; in: Physiology and pathobiology of axons, pp. 3–64. Ed. S.G. Waxman. Raven Press, New York 1978.

4 Berthold, C.-H., Some aspects on the ultrastructural organization of peripheral myelinated axons in the cat; in: Proc. Life Sciences; Axoplasmic transport, pp. 40–54. Ed. D.G. Weiss. Springer, Berlin/Heidelberg/New York 1982.

5 Berthold, C.-H., and Rydmark, M., Electron microscopic serial section analysis of nodes of Ranvier in lumbosacral spinal root of the cat: ultrastructural organization of nodal compartments in fibers of different sizes. J. Neurocyt. *12* (1983) 475–505.

6 Berthold, C.-H., and Rydmark, M., Electron microscopic serial section analysis of nodes of Ranvier in lumbosacral spinal roots of the cat: paranodal Schwann cell mitochondria. In manuscript.

7 Berthold, C.-H., Corneliuson, O., and Rydmark, M., Changes in shape and size of cat spinal root myelinated nerve fibers during fixation and Vestopal-W embedding for electron microscopy. J. Ultrastr. Res. *80* (1982) 23–41.

8 Berthold, C.-H., Rydmark, M., and Corneliuson, O., Estimation of sectioning compression and thickness of ultrathin sections through Vestopal-W embedded cat spinal roots. J. Ultrastr. Res. *80* (1982) 42–52.

9 Chiu, S.Y., Asymmetry currents in the mammalian myelinated nerve. J. Physiol. *309* (1980) 499–519.

10 Coppin, C.M.L., and Jack, J.J.B., Internodal length and conduction velocity of cat muscle afferent nerve fibers. J. Physiol. *222* (1972) 91P–93P.

11 Cullheim, S., Relations between cell body size, axon diameter and axon conduction velocity of cat α-motoneurons stained with horseradish peroxidase. Neurosci. Let. *8* (1978) 17–20.

12 Cullheim, S., and Kellerth, J.-O., A morphological study of the axons and recurrent axon collaterals of cat α-motoneurones supplying different functional types of muscle unit. J. Physiol. *281* (1978) 301–313.

13 Ellisman, M.H., Friedman, P.L., and Hamilton, W.J., The localization of sodium and calcium to Schwann cell paranodal loops at nodes of Ranvier and calcium to compact myelin. J. Neurocyt. *9* (1980) 185–205.

14 Erlanger, J., and Blair, E.A., Comparative observation of motor and sensory fibers with special reference to the repetitiousness. Am. J. Physiol. *121* (1938) 431–453.

15 Ghabriel, M.N., and Allt, G., The node of Ranvier; in: Progress in anatomy, vol. 2, pp. 137–160. Eds R.J. Harrison and V. Navaratnam. Cambridge University Press, Cambridge 1982.

16 Hall, S.M., and Wiliams, P.L., The distribution of electron-dense tracers in peripheral nerve fibers. J. cell Sci. *8* (1971) 541–555.

17 Hirano, A., and Dembitzer, H.M., Morphology of normal central myelinated axons; in: Physiology and pathobiology of axons, pp. 65–82. Ed. S.G. Waxman. Raven Press, New York 1978.

18 Landon, D.N., Structure of normal peripheral myelinated nerve fibers; in: Advances in neurology, vol. 31. Demyelinating diseases, Basic and clinical electrophysiology, pp. 25–49. Eds S.G. Waxman and J.M. Ritchie. Raven Press, New York 1981.

19 Landon, D.N., and Hall, S., The myelinated nerve fiber; in: The peripheral nerve, pp. 1–105. Ed. D.N. Landon. Chapman and Hall, London 1976.

20 Langley, O.K., Histochemistry of polyanions in peripheral nerve; in: Complex Carbohydrates of Nervous Tissue, pp. 193–207. Eds R.U. Margolis and R.K. Margolis. Plenum Press, New York and London 1979.

21 Livingstone, R.B., Pfenninger, K., Moor, H., and Akert, K., Specialized paranodal and interparanodal glial-axonal in the peripheral and the central nervous system: a freeze-etching study. Brain Res. *58* (1973) 1–24.

22 Loud, A.V., A quantitative stereological description of the ultrastructure of normal rat liver parenchymal cells. J. cell Biol. *37* (1968) 27–46.

23 Neumcke, B., and Stämpfli, R., Sodium currents and sodium-current fluctuations in rat myelinated nerve fibers. J. Physiol. *329* (1982) 163–184.

24 Neumcke, B., Schwarz, W., and Stämpfli, R., Differences between K channels in motor and sensory nerve fibers of the frog as revealed by fluctuation analysis. Pflügers Arch. *387* (1980) 9–16.

25 Rosenbluth, J., Freeze-fracture approaches to ionophore localization in normal and myelin-deficient nerves; in: Advances in neurology, vol. 31, Demyelinating diseases, Basic and clinical electrophysiology, pp. 391–418. Eds S.G. Waxman and J.M. Ritchie. Raven Press, New York 1981.

26 Rydmark, M., Nodal axon diameter correlates linearly with internodal axon diameter in spinal roots of the cat. Neurosci. Lett. *24* (1981) 247–250.

27 Rydmark, M., and Berthold, C.-H., Electron microscopic serial section analysis of nodes of Ranvier in lumbar spinal roots of the cat: a morphometric study of nodal compartments in fibers of different sizes. J. Neurocytol. *12* (1983) 537–565.

28 Schnapp, B., and Mugnaini, E., Membrane architecture of myelinated fibers as seen by freeze-fracture; in: Physiology and pathobiology of axons, pp. 83–123. Ed. S.G. Waxman. Raven Press, New York 1978.

29 Seneviratne, K.N., Peiris, O.A., and Weerasuriya, A., Effects of hyperkalaemia on the excitability of peripheral nerve. J. Neurol. Neurosurg. Psychiat. *35* (1972) 149–155.

30 Skoglund, C.R., The responce to linearly increasing currents in mammalian motor and sensory nerves. Acta physiol. scand. *4* (1942) suppl. 12.

31 Spencer, P.S., and Thomas, P.K., Ultrastructural studies of the dying-back process. II. The sequestration and removal by Schwann cells and oligodendrocytes of organelles from normal and diseased axons. J. Neurocytol. *3* (1974) 763–783.

32 Stämpfli, R., Overview of studies on the physiology of conduction in myelinated nerve fibers; in: Advances in neurology, vol. 31, Demyelinating diseases, Basic and clinical electrophysiology, pp. 11–23. Eds S.G. Waxman, and J.M. Ritchie. Raven Press, New York 1981.

33 Stämpfli, R., and Hille, B., Electrophysiology of the peripheral myelinated nerve; in: Frog neurobiology, pp. 3–32. Eds R. Llinas and W. Precht. Springer, Berlin/Heidelberg/New York 1976.
34 Tao-Cheng, J.-H., and Rosenbluth, J., Nodal and paranodal membrane sturcture in complementary freeze-fracture replicas of amphibian peripheral nerves. Brain Res. *199* (1980) 249–265.
35 Vallbo, Å.B., Accomodation related to inactivation of the sodium permeability in single myelinated nerve fibers from *Xenopus laevis*. Acta physiol. scand. *61* (1964) 429–444.
36 Waxman, S.G., and Foster, R.E., Ionic channel distribution and heterogeneity of the axon membrane in myelinated fibers. Brain Res. Rev. *2* (1980) 205–234.
37 Wiley, C.A., and Ellisman, M.H., Rows of dimeric-particles within the axolemma and juxtaposed particles within glia, incorporated into a new model for the paranodal glial-axonal junction at the node of Ranvier. J. Cell Biol. *84* (1980) 261–280.

0014-4754/83/090964-13$1.50+0.20/0

VII. The myelinated nerve: Some unsolved problems

by B. Neumcke

I. Physiologisches Institut, Universität des Saarlandes, D-6650 Homburg/Saar (Federal Republic of Germany)

The previous chapters of this multi-author review have illustrated that the electrophysiological and morphological properties of myelinated nerve fibers are intimately related. For example, the kinetics of drug action described in the chapter by Ulbricht cannot be interpreted without a detailed knowledge of the nodal architecture (see the contribution by Berthold and Rydmark), and the identification of intramembranous nodal particles with ionic channels as suggested by Rosenbluth would be very vague without the determination of channel numbers from electrophysiological measurements (compare the section by Schwarz). In the following we want to list some properties of myelinated nerve fibers which are not yet fully understood and which may be elucidated by future electrophysiological and morphological investigations.

Myelinated nerve fibers may be classified according to their function (motor or sensory fiber) or according to their origin (amphibian or mammalian fiber). All different types of fibers exhibit different conduction properties. These electrophysiological differences are not only apparent in the various shapes of the action potentials but are already expressed by different ionic permeabilities in the resting state. Thus the resting potassium conductance of a frog motor fiber is larger than the one of a sensory fiber while the magnitude of the resting potential is comparable in both cases[10].

Significant differences in the generation of resting potentials also seem to exist between amphibian and mammalian myelinated nerve fibers: For frog nerve fibers the resting potential in Ringer's solution containing 2.5 mM K^+ ions is −71 mV at 17 °C as measured with a 'cover-slip' method[5]. Figure 1 shows the determination of the resting potential of a single rat myelinated nerve fiber by a similar technique (for details see the legend). At a temperature of 21 °C the resting potential of the fiber was only −50 mV and no action potentials could be elicited from this level not even by strong depolarizing current pulses. Hence the resting potential in vivo must be more negative and it is then probably not controlled entirely by passive ionic membrane permeabilities. The temperature dependence of the resting potential of the isolated rat nerve fiber (fig. 1) also suggests that active metabolic processes may be decisive in the function of mammalian myelinated nerve fibers. On the other hand, no such pronounced effect of temperature on the resting potential of isolated frog myelinated nerve fibers could be observed (B. Neumcke and R. Stämpfli, unpublished).

The most striking difference between amphibian and mammalian nerve fibers is the virtual absence of

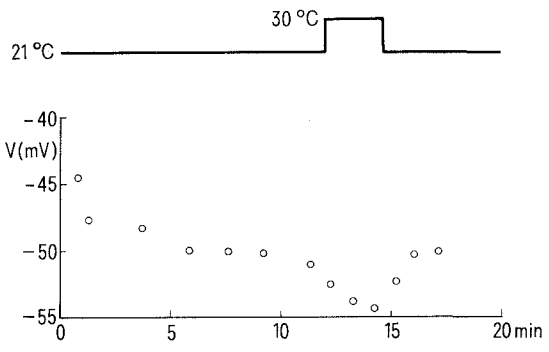

Figure 1. Resting potential V of a single myelinated fiber from a rat sciatic nerve. A 4–5 mm section of the fiber with adherent nerve trunks on both sides was mounted in the recording chamber in which all compartments were flooded with extracellular solution. The fluid level was then lowered until the compartments were separated from each other. The compartment containing the test node (A pool) remained filled with flowing extracellular solution whereas the solution in the neighboring pools was replaced by isotonic KCl. In one of these side compartments (C pool) the fiber was cut beyond the neighboring node. The resting potential V of the test node was then determined as the voltage from an external source between pools A and C at which no injury current between A and C could be detected. Symbols represent measurements of V at various times after cutting the fiber in the C pool. Note the reversible decrease of V after a temperature increase of the extracellular solution from 21 to 30 °C. The extracellular solution contained 154 mM NaCl, 2.2 mM $CaCl_2$, 5.6 mM KCl and 10 mM morpholinopropanesulphonic acid at pH 7.2. Isotonic KCl solution was composed of 155 mM KCl, 5 mM NaCl and 10 mM morpholinopropanesulphonic acid at pH 7.2. Experiment 42/82 (Neumcke and Stämpfli, unpublished).